

Use of a Laser Scanner System for Precise Roll Surface Mapping

1.0 INTRODUCTION

Many industries use processes in which material must pass over one or more machine rolls. Two common examples are the paper making and printing industries. In both cases, the shape and roughness of the machine roll is a crucial factor in the processing of the paper. For example, if the dihedral angle of a guide roll is not correct, the paper may bunch up or roll off of the roll, thus halting production. Similarly, a warped roll can adversely affect the quality of the paper produced. The same principle applies to the alignment of the rolls, since paper can break if two rolls are not parallel within certain tolerances (Sprenst and Hudson, 1996).

As machine speeds increase, the tolerances on the shape and orientation of rolls become ever more stringent. In addition, increased production outputs drive up the costs associated with the down-time required to survey a suspect roll. This makes the development of fast, cost-effective methods to accurately determine roll shape and orientation very attractive to industry.

This paper presents the results of research aimed at the production of a precise (sub-millimetre), non-contact method of roll mapping based on the use of a 3D auto-synchronous laser scanner. It is a new method that provides both the deviations *on the entire surface* of the roll *and* the orientation of the roll itself, but only requires a single setup using a Laser Scanning System.

2.0 ROLL MAPPING WITH A LASER SCANNER SYSTEM

The critical features of a machine roll are its orientation with respect to other rolls in a machine train and the shape of the roll's surface. In most surveys, these two features are determined by separate methods. However, by using a laser scanner to provide three dimensional coordinates of elements on the roll's surface, both features can be simultaneously determined.

Generally, laser scanner systems are measurement devices designed to provide three-dimensional coordinates on a surface by illuminating surface elements using a coherent monochromatic light source. In particular, auto-synchronous laser scanners are a class of scanners that are capable of high data rates (up to 18 kHz), high sampling density and are relatively insensitive to lighting conditions. As a result, the authors investigated the possibility of using an auto-synchronous laser scanner to map machine rolls.

Figure 1 illustrates the principle of auto-synchronization. A double-sided mirror deflects both the emitted laser beam and the optical axis of the receiving lens onto two fixed mirrors, which then deflect the paths again such that they intersect outside the scanner. As shown in figure 2, the optically "unfolded" system is derived by tracing the optical projection of the lens, sensor and laser through the mirrors. Note that as shown, only two dimensions can be scanned – a third is possible by including a second mirror to deflect the optical paths out of the page.

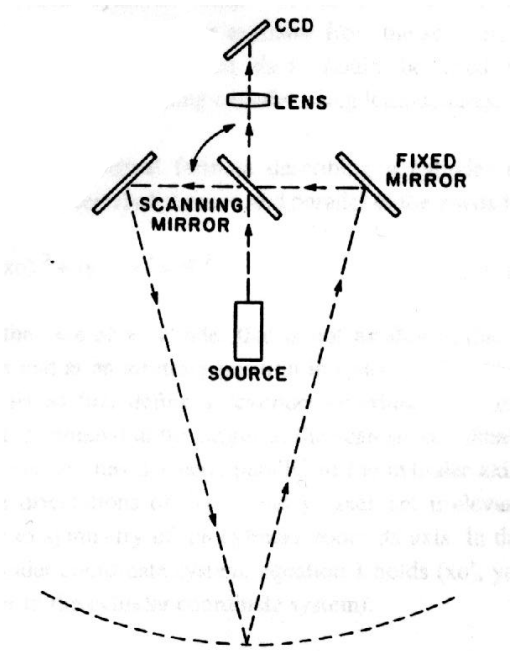


Figure 1. Principle of Auto-synchronization
(from Blais et al, 1988)

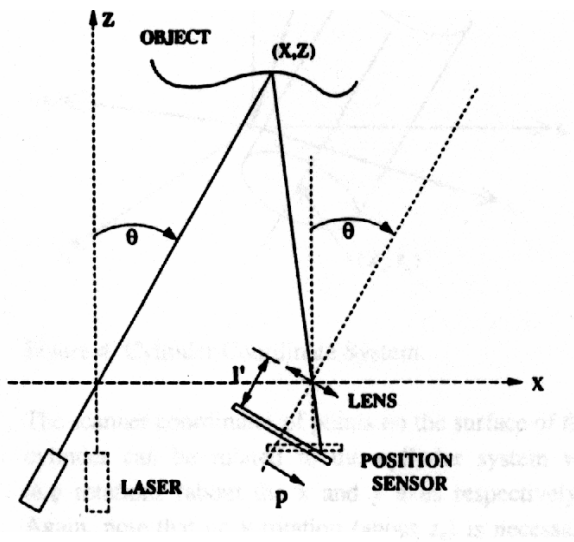


Figure 2. Optically Unfolded System
(from Blais et al, 1988)

For a given rotation of the mirror θ , there are an infinite number of possible x, z coordinate pairs that the laser path passes through. However, when a particular surface element intersects the path, it is imaged on the CCD array at unique point p . Thus for a given p, θ combination, the

x, z coordinates of the surface element can be calculated if the location and orientation of all the optical elements are known.

In addition, the CCD array does not only record the position at which the laser spot is imaged, but also the intensity of the reflection. As a result, two images are produced, a depth image of the scene and an intensity image, analogous to a black and white photograph. A pair of images for a scene is shown in figure 3.

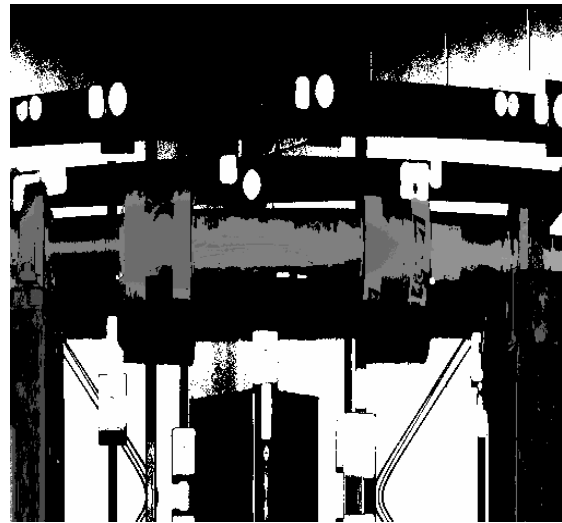


Figure 3. Laser Scanner Output. The top image is a depth image, while the bottom image is the corresponding intensity image.

3.0 ELEMENTS OF THE SURFACE MAPPING SYSTEM

The process of transforming a scanned image of a roll into a digital elevation map of the roll's surface can be broken down into five main parts, namely:

1. Data Acquisition
2. Data Transformation
3. Determination of Roll Parameters
4. Projection onto the Mapping Plane
5. Re-sampling into a Digital Map

As a result, the mapping system developed is actually a collection of separate modules that interact sequentially as shown in figure 4.

3.1 Data Acquisition and Preprocessing

As mentioned in section 2, the laser scanner returns two raster images – a depth file and an intensity file. However, this data must be preprocessed before a map of the imaged roll surface can be generated.

A typical image acquired from a laser scanner is shown below in figure 5. In every such image, there are portions that correspond to useable data on the roll surface (A), non-usable data on the roll surface (B) and background (C).

Background areas are those which do not correspond to the roll surface at all (labeled C in the below image). This includes imagery of surrounding machinery, the floor and anything else that is not part of the roll..

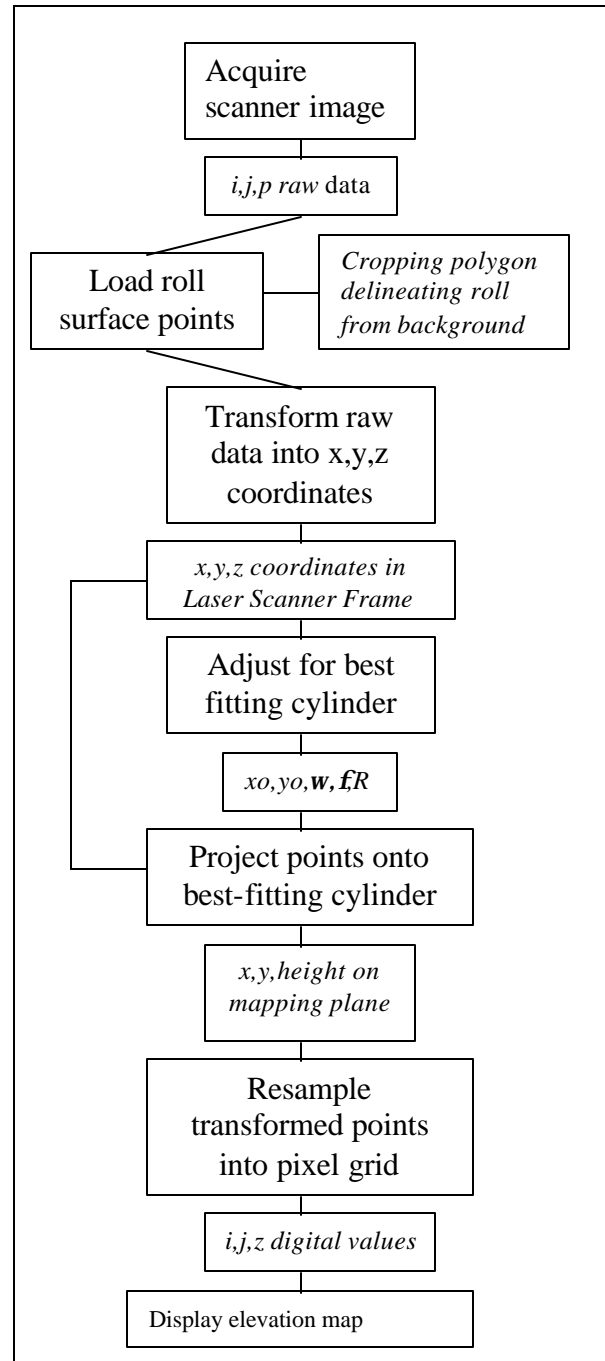


Figure 4. System Flowchart. Data is in italics while processes are in regular type.

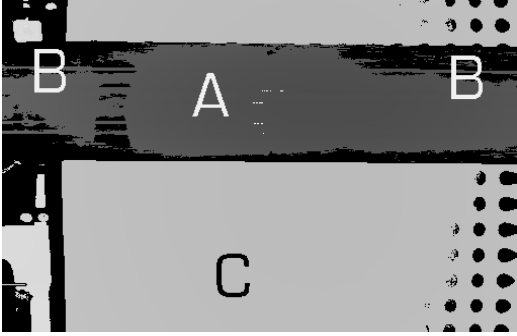


Figure 5. Typical areas of a roll showing useable roll area (A), non-useable roll area (B) and background (C).

Non-useable roll areas are those roll surface elements which the laser scanner illuminates, but does not receive a useable return signal from. This can either be due to insufficient signal return to the receiver, or oversaturation of the CCD array due to direct reflection from a highly reflective surface.

Since a raw image has no intrinsic semantic content, additional information is required to segment an image into background and roll areas. This is accomplished by defining a *cropping polygon* which encloses the roll area.

Once the cropping polygon has been defined, the system then uses an “escape route” point-in-polygon search (Burrough, 1994) to check whether a given scanned point lies within the cropping polygon. The system then loads all useable points into memory.

3.2 Data Transformation

Once the useable data has been loaded, it must be converted from the i,j,p (image frame) system into an x,y,z Cartesian system. Specifically, the data is transformed to the Cartesian system shown in figure 6. As can be seen, the system has its origin at the *optical center* of the laser scanner. The z -axis extends away from the scanner and is parallel to the bisector of the angle

subtended by the emitted ray and the received ray when the mirror angles are zero and a zero p -value is read. The x -axis then lies in the average plane swept out by the laser for a constant value of α . Finally, the y axis is orthogonal to the z and x axes to form a *left-handed* system.

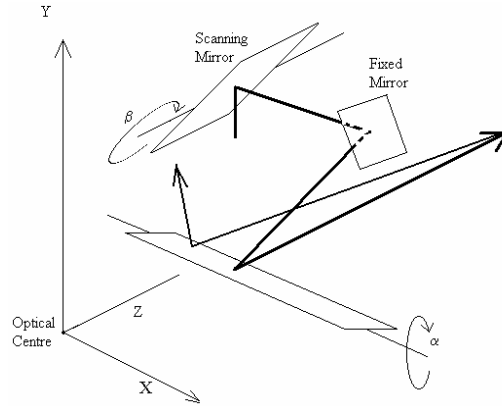


Figure 6. Axes of the laser scanner system.

It is important to note that the i,j,p system is not exactly equivalent to the spherical system (azimuth, zenith, distance) familiar to most. The p value measured is not a direct measure of the distance of a surface element from the scanner. Also, due to the scan geometry, as well as irregularities in the galvanometers used to drive the scanning mirrors, equal increments of i or j do not correspond to equal changes in the direction to a surface element from the center of the scanner. As mentioned previously, the relationship between i,j,p and x,y,z is very complicated and will not be presented here. In addition, irregularities in mirror shapes, lens distortions and optical element placement make calibration of this device very complicated (see Al-Hanbali, 1998 for details). The system uses an early set of calibration parameters developed by Dr. Al-Hanbali over the course of his work on calibration of the NRC scanner.

3.3 Determination of roll parameters

Prior to generating a contour map of a roll surface, some datum surface must be defined. A contour map then describes the deviations of the actual roll surface from this theoretical reference. Using a cylinder as a datum is natural since this is the shape that a roll nominally takes.

The problem remaining is how to determine this reference cylinder. Since coordinates of surface elements on the roll are available from the scanner, it seems natural that this data should be used to determine a best-fitting cylinder using least-squares.

The mathematical formula describing a cylinder of radius R , centered at x_0, y_0 and parallel to the z -axis is

$$(x-x_0)^2 + (y-y_0)^2 = R^2 \quad (\text{eq. 1})$$

In the case of a cylinder that is not parallel to the z -axis and at an arbitrary position in space (as in figure 3), let us first define a “cylinder coordinate system” that is centered at the origin of the scanner coordinate system and has a z' -axis parallel to the cylinder axis. The orientations of the x' and y' axes are irrelevant due to symmetry of the cylinder about its axis. In the cylinder coordinate system, equation 1 holds (x_0', y_0' refer to the cylinder coordinate system).

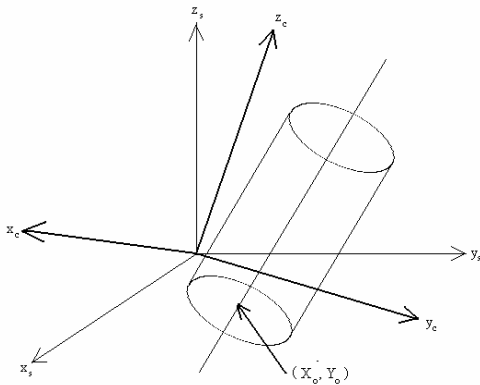


Figure 3. Cylinder Coordinate System.

The scanner coordinates of points on the surface of the cylinder can be rotated to the cylinder system via ω, ϕ rotations (about the x and y axes respectively). Again, note that no κ rotation (about z_c) is necessary due to rotational symmetry.

The explicit form of this rotation matrix is:

$$\begin{bmatrix} x' \\ y' \\ z' \end{bmatrix} = R_y(\mathbf{j}) \cdot R_x(\mathbf{w}) \cdot \begin{bmatrix} x \\ y \\ z \end{bmatrix} \quad (\text{eq. 2})$$

$$= \begin{bmatrix} \cos \mathbf{j} & \sin \mathbf{w} \sin \mathbf{j} & -\sin \mathbf{f} \cos \mathbf{w} \\ 0 & \cos \mathbf{w} & \sin \mathbf{w} \\ \sin \mathbf{j} & -\sin \mathbf{w} \cos \mathbf{j} & \cos \mathbf{j} \cos \mathbf{w} \end{bmatrix} \cdot \begin{bmatrix} x \\ y \\ z \end{bmatrix}$$

If the expressions for x', y' are substituted into eq. 2, we obtain the mathematical relationship between points on the cylinder *in scanner space*, vis. ,

$$(x \cos \mathbf{j} + y \sin \mathbf{w} \sin \mathbf{j} - z \sin \mathbf{j} \cos \mathbf{w} - x_0')^2 + (y \cos \mathbf{w} + z \sin \mathbf{w} - y_0')^2 - R^2 = 0 \quad (\text{eq. 3})$$

Thus a cylinder is completely defined by five parameters – radius, two rotations to define orientation, and two translations to define location. Given a set of n (x, y, z) coordinates on the surface of the cylinder, n equations of the form of eq. 3 can be written, and the parameters can be solved for via an implicit, non-linear least-squares adjustment.

3.4 Projection onto the reference cylinder

Once the best-fitting cylinder parameters have been determined, an elevation map describing the deviations of the scanned surface elements from this surface can be created.

To generate a map of the roll surface, a graticule on the reference cylinder is defined by the intersection of the cylinder with planes normal to the cylinder axis (latitude) and by lines parallel to the axis on the cylinder surface (longitude). Note that since the cylinder has curvature in only one direction, the graticule can be mapped into a plane with no distortion. For convenience, the y-axis is defined to be coincident with the line of latitude corresponding to the end of the cylinder, while the x-axis is coincident with the long edge of the scanned roll area.

The task remaining is to find the latitude and longitude of each surface element scanned and to calculate the height of the element above or below the reference cylinder.

This can be accomplished via the following procedure:

1. Transform a point into the cylinder coordinate system using the solved orientation and location of the reference cylinder via

$$\begin{bmatrix} x_p' \\ y_p' \\ z_p' \end{bmatrix} = R_y(\mathbf{j}) \cdot R_x(\mathbf{w}) \cdot \begin{bmatrix} x_p \\ y_p \\ z_p \end{bmatrix} - \begin{bmatrix} xO' \\ yO' \\ 0 \end{bmatrix} \quad (\text{eq. 4})$$

2. Calculate the latitude, longitude, and height of the point from

$$Lat = z_p' \quad (\text{eq. 5})$$

$$Long = R \cdot \tan^{-1}\left(\frac{x_p'}{y_p'}\right) \quad (\text{eq. 6})$$

$$Height = \sqrt{(x_p')^2 + (y_p')^2} - R \quad (\text{eq. 7})$$

3. Repeat steps 1 and 2 for all the scanned points.

The result of this module is an array of spot heights above and below the reference cylinder

with associated mapping plane coordinates (lat,long).

3.5 Generation of an Elevation Map

Spot elevations of irregularly distributed points on the surface of the roll are not generally useful since they convey *too much* information to a human interpreter. Rather, such information is much more useful if it can be generalized into contours or shaded plots. These allow trends in the surface to be readily apparent. For simplicity, the system generates a shaded elevation map. However, this requires re-sampling of the irregularly distributed spot data into a grid.

The weighted-distance resampling method (MacDougal, 1976) is a simple resampling method that only uses a local neighbourhood of data points surrounding the pixel location. This assumes that each point has a finite area over which it has influence, which is a function of its distance to other points (analogous to a covariance function that goes to zero at a finite separation distance). The advantages of this method is that it is very simple to implement, provides good results, and limits the influence area to one pixel distance. Thus each sample will affect a maximum of four pixels, limiting the amount of processing required.

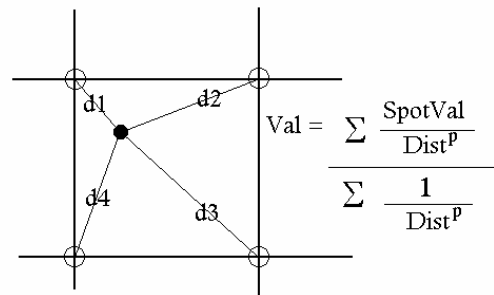


Figure 4. Weighted distance resampling.

The principle of weighted distance interpolation is illustrated in figure 18. The value of each data point is “distributed” to the nearest four pixels

according to the distance the pixel is from the data point. The value of p dictates the characteristics of the resampling. For example, higher values of p mean that the influence of a data point decays more quickly, but that pixels are most affected by the nearest data point (in the limit, this becomes a nearest neighbour interpolator). Thus, lower values of p act as smoothers, while higher values act as enhancers.

Once the spot data has been resampled into a regular grid, the elevations are quantized between 0-256 for output as a greyscale image. Of course, the original range of elevations are retained to allow for later quantitative analysis.

4.0 TESTING RESULTS

Once the mapping system modules were completed and individually tested, the authors performed a series of tests to check the performance of the system as a whole. The tests presented here are:

1. Scan of a Vertical Sonotube
2. Scan of a Horizontal Sonotube
3. Scan of a Roll with Controlled Surface Distortions

The results and significance of the above tests are discussed in the following sections.

4.1 Scan of a Vertical Sonotube

The first test involved the scan of a vertical cylinder. The cylinder was a 9" (nominal) diameter rigid cardboard tube. The surface of the roll is fairly smooth, but has sub-millimetre helical ridges running along the length of the tube as a result of the manufacturing process. The tube was placed approximately 80cm away from the scanner (in the optimal scan zone). This yielded 61 629 points to process.

The results of the adjustment are shown below in table 1.

Table 1. Adjustment Results for Vertical Sonotube

Parameter	Adjusted Solution	Standard Deviation
Xo	837.41 mm	0.05 mm
Yo	71.79 mm	0.01 mm
ω	-179.0°	18.0 "
ϕ	-18.8°	7.6 "
R	103.11 mm	0.05 mm

Note that the standard deviations in the above cases are extremely small. The authors believe that this is an overly optimistic estimate of the accuracy of the solutions since the actual values of the solution can vary significantly once the number of points is lowered even slightly. The extreme number of points is the culprit for this since neighbouring points contribute very little information due to high correlation – a fact not contained in the diagonal covariance matrix used. Thus the redundancy of (61629-5) is misleading. To be rigorous, a covariance function should be calculated for the data and a CI matrix with off diagonal elements used in the adjustment.

Also, note that the radius of 103 mm is significantly off of the nominal radius of 100mm as measured with a steel scale. This is due to the low degree of arc measured, resulting in a large correlation between the radius and x_0 parameters.

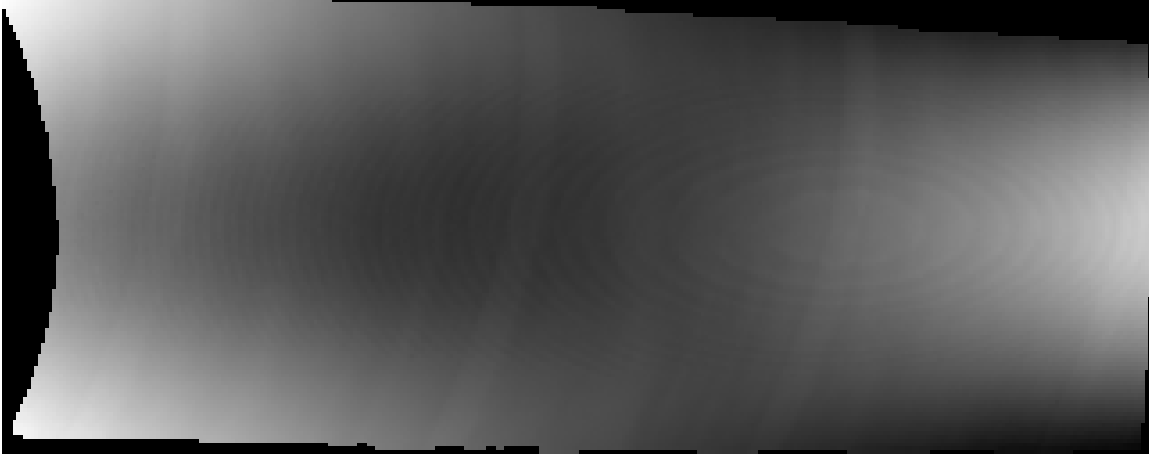


Figure 7. Elevation map for the vertical sonotube.

Despite this finding, an elevation map was generated for the roll. This is shown in figure 7. Note the systematic nature of the elevation changes in the image. This pattern could be due to an actual deformation of the roll, or a systematic error in the laser scanner measurements. To check for a systematic error in the scanner, the roll was rotated by 180° and re-scanned. Exactly the same distortion pattern resulted. As a result, the presence of a scanner systematic error was suspected.

6.2 Scan of a Horizontal Sonotube

To check for a scanner error, the authors repeated the experiment in section 5.1, but placed the sonotube in a horizontal position. If the tube was truly deformed, the same distortions would be seen in the horizontal maps as in the vertical maps. However, if the distortion pattern changed, a scanner systematic error would be confirmed.

The adjustment results from the horizontal test are contained in table 2.

Table 2. Adjustment Results for Horizontal Sonotube

Parameter	Adjusted Solution	Standard Deviation
Xo	1015.78 mm	0.04 mm
Yo	20.14 mm	0.01 mm
ω	176.6°	15.4 "
ϕ	0.1°	6.4 "
R	112.96 mm	0.05 mm

Note that the radius is significantly different between the two tests, despite the same roll being used. As mentioned, this is due to the high correlation between the xo and R parameters.

Figure 8 shows the elevation map for the roll. The diagonal lines are the effects of the sub-millimetre ridges on the surface of the sonotube.

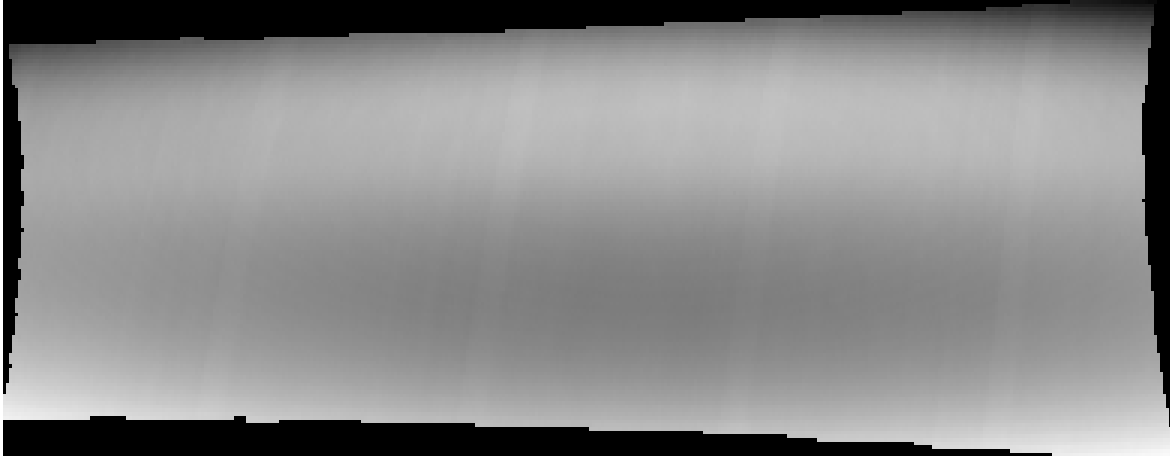


Figure 8. Elevation Map of Horizontal Sonotube.

Note that the horizontal roll showed much less distortion than the vertical. This implies that the scanner has a systematic error in the vertical direction. Al-Hanbali (1998) confirms this discovery and presents a modified set of calibration results that should eliminate this systematic error. However, the authors have yet to test these results.

Scan of a Roll with Controlled Surface Distortions

Another test performed was to scan a roll with known surface distortions. Since it is very difficult to actually measure the distortions of a

surface using any conventional method, the authors attached several pieces of wire of known diameter to a 4" plastic pipe. The same procedure was followed in this test as for that of the smooth sonotube. The corresponding elevation map of the roll is shown in figure 8. Quadratic weighting was used to better preserve the high frequency information at the wire edges.

Note that the dark "holes" in the elevation map are areas where either specular reflection occurred off the wires or spots the scanning beam could not illuminate due to shadow effects.

To quantitatively analyse the accuracy of the system in measuring distortions in the roll surface, five cross sections across the wire paths

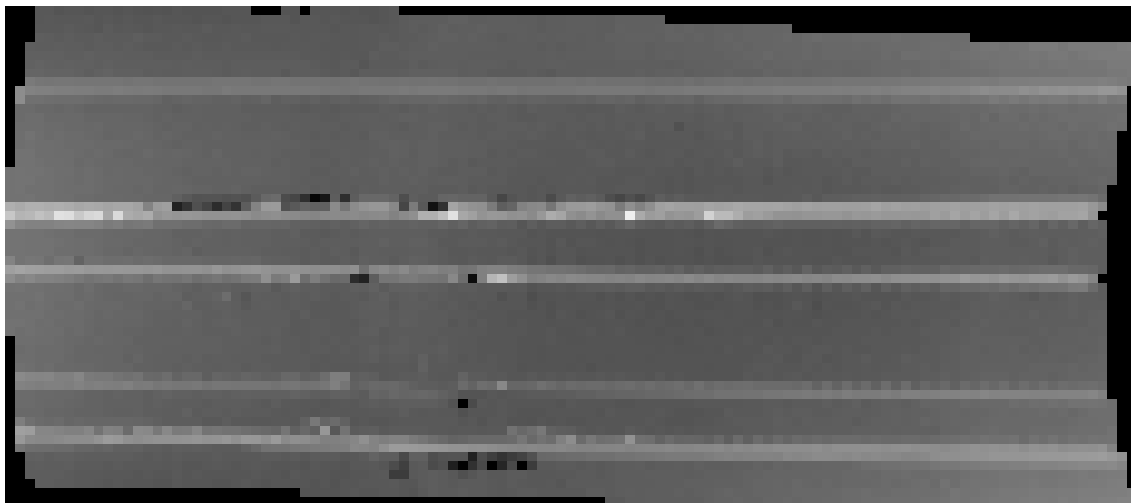


Figure 9. Elevation Map of Control Surface.

Pixel Variation along Surface of Wired Roll using Quadratic Weighting

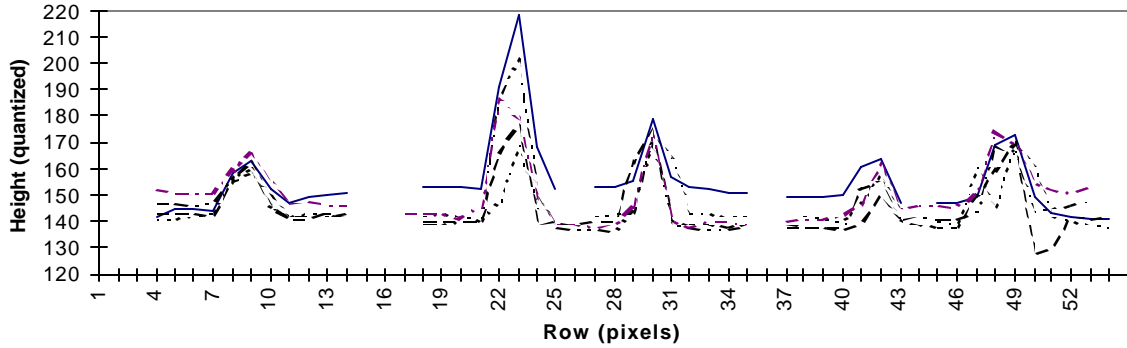


Figure 6. Cross-sections from wired roll

were taken and plotted in figure 9. Surprisingly, the large wire proved to be the least consistent. This is due to noise from specular reflection and shadow effects as mentioned above.

Finally, the average wire diameter was calculated for each wire using the cross sectional data. Points for each cross section on either side of the peak were averaged to provide a “base” gray scale elevation. The peak value in each cross-section was then averaged to provide the “peak” greyscale elevation. These were then converted to linear units via

$$Diameter = (z_{peak} - z_{base}) \cdot \frac{H_{high} - H_{low}}{256 - 10} \quad (\text{eq. 8})$$

where H_{high} , H_{low} ... highest and lowest elevations on the map

These are compared to the measured diameters in Table 2. The reference diameters were determined by measuring the wire diameter in three positions with a digital micrometer (least count 0.01 mm) and averaging the set.

Table 2. Analysis of Scanner Wire Diameters

Wire	Measured Diameter (mm)	Scanned Diameter (mm)	Error (mm)
1	1.000	0.961	0.039
2	2.420	2.431	0.011
3	1.580	1.740	0.160
4	1.000	0.999	0.001
5	1.530	1.482	0.048
	Mean		0.052

As can be seen, this mapping system is definitely capable of resolving small surface deviations extremely accurately. This is especially significant when one considers that the width of the structure measured is on the order of a few millimetres.

5.0 Conclusions

The mapping system developed here was a proof-of-concept endeavor. As is, the system will take in a laser scanner image of a roll and determine the parameters of the best-fitting cylinder given minimal user input. A greyscale elevation map of the visible surface of the roll is then automatically generated. Thus, the authors are confident that the basis of an operational roll mapping system has been established. This system is able to perform roll surveys in a fraction of the time required by conventional methods. In addition, the greyscale map is a feature previously unachievable by any method.

In particular, the system shows great promise in detecting small variations in a roll surface. The appearance of the ridges in the sonotube maps and the accuracy of the wire gauge determination are proof of this.

The accuracy of the roll determination is the weak point in the system. Unfortunately, this is primarily due to the limited degree of arc observed. Future work should focus on effectively meshing several views of the roll in different rotational positions, probably using targets on the roll and the intensity file supplied.

As well, there remain unresolved systematic distortions in the laser scanner measurements, in particular in the vertical direction. Although the distortions do not seem to affect the resolution of very small deformations (i.e. on the mm scale), the authors feel that these distortions limit the usefulness of using the scanner to measure large scale deformations, such as thermal growth in industrial equipment.

However, the authors are satisfied that the objectives of this study were accomplished. A non-contact, fast method of static roll mapping

was developed using a 3D auto-synchronous laser scanner. This system shows great promise in industrial applications provided a better understanding of the error characteristics of the scanner is gained.